Cell Reports
Physical Science

Article

Contrasting a BYD Blade prismatic cell and Tesla 4680 cylindrical cell with a teardown analysis of design and performance

Graphical abstract

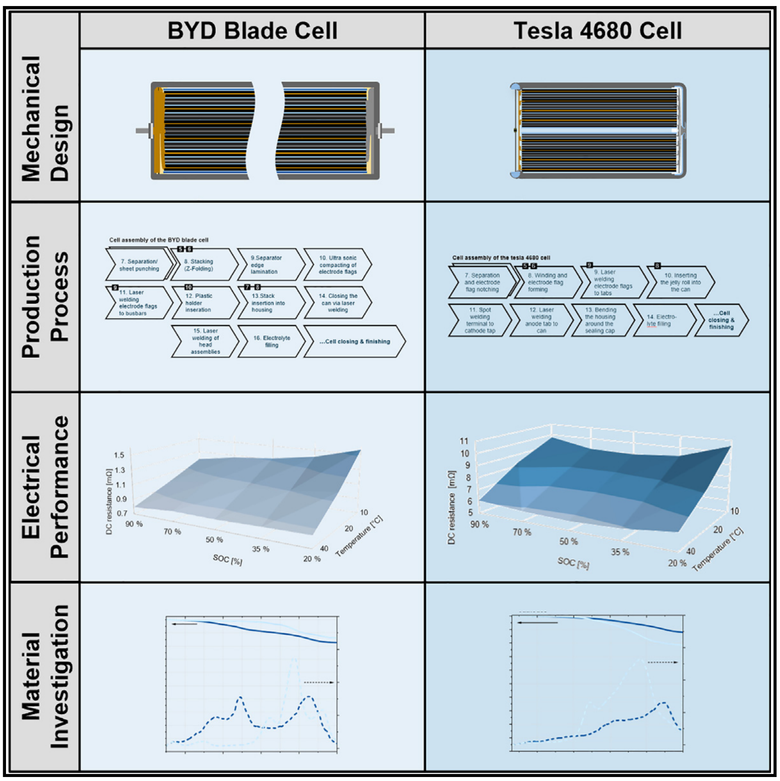

Highlights

- Design, materials, performance, and process flow of BYD Blade and Tesla 4680 cell are compared
- Tesla uses laser welding; BYD combines laser and ultrasonic for electrode connections
- Tesla 4680 cell generates 2× the heat per volume of BYD Blade at a 1 C specific load
- PAA and PEO binders identified in Tesla 4680 anode warrant further investigation

Authors

Jonas Gorsch, Julius Schneiders, Moritz Frieges, ..., Achim Kampker, Marina Muñoz Castro, Eleonore Siebecke

Correspondence

j.gorsch@pem.rwth-aachen.de (J.G.), m.frieges@pem.rwth-aachen.de (M.F.)

In brief

Gorsch et al. compare BYD Blade and Tesla 4680 cells. The Blade cell (LFP) excels in efficiency, while the 4680 cell (NMC811) offers higher energy density and a tabless design. Key differences in design, materials, and performance reveal trade-offs, providing a reference point for future lithium-ion battery innovation.

Gorsch et al., 2025, Cell Reports Physical Science 6, 102453
March 19, 2025
https://doi.org/10.1016/j.xcrp.2025.102453

CellPress

Cell Reports
Physical Science

CellPress
OPEN ACCESS

Article

Contrasting a BYD Blade prismatic cell and Tesla 4680 cylindrical cell with a teardown analysis of design and performance

Jonas Gorsch,[1,4,*] Julius Schneiders,[1] Moritz Frieges,[1,*] Niklas Kisseler,[1] Domenic Klohs,[1] Heiner Heimes,[1] Achim Kampker,[1] Marina Muñoz Castro,[2] and Eleonore Siebecke[3]

[1]Production Engineering of E-Mobility Components (PEM), RWTH Aachen University, Aachen, Germany
[2]MEET - Münster Electrochemical Energy Technology, University of Muenster, Muenster, Germany
[3]Fraunhofer Institute for Ceramic Technologies and Systems IKTS, Dresden, Germany
[4]Lead contact
*Correspondence: j.gorsch@pem.rwth-aachen.de (J.G.), m.frieges@pem.rwth-aachen.de (M.F.)
https://doi.org/10.1016/j.xcrp.2025.102453

SUMMARY

In order to provide design guidance for the development of next-generation batteries, this article presents a teardown analysis of two commercial lithium-ion batteries: the Tesla 4680 cell and the BYD Blade cell. Insights into these cells' electrical, mechanical, material, and process designs are provided. The BYD Blade cell displays half the energy losses per volume of the Tesla 4680 cell at the same C-rate. The Tesla 4680 cell utilizes laser welding, and the BYD Blade cell utilizes laser and ultrasonic welding as electrode contacting technologies. Lithium iron phosphate (LFP; BYD Blade cell) and NMC811 (Tesla 4680 cell) are confirmed as electrode materials resulting in energy densities of 160 Wh/kg and 355.26 Wh/l and 241.01 Wh/kg and 643.3 Wh/l, respectively, on the cell level. Both cells utilize graphite anodes without silicon dioxide. Polyacrylic acid (PAA) and polyethylene oxide (PEO) are detected as binders on the anode side for the Tesla 4680 cell. A manufacturing sequence is proposed for both cells.

INTRODUCTION

In 2023, two manufacturers dominated the market for battery electric vehicles (BEVs) based on sold vehicles.[1] Tesla, a pioneer in using lithium-ion batteries (LIBs), led sales in Europe and North America in 2023. Meanwhile, BYD, which began as a battery cell manufacturer, has become a leader in innovation from cell to vehicle level and has gained significant market share for sold BEVs worldwide. In 2024 BYD surpassed Tesla in total BEV sales.[2] In 2022, Tesla began producing 4680 cylindrical cells in California and Texas (USA) and sourced prismatic cells from CATL. The Tesla 4680 cells are approximately five times larger by volume and capacity than the previously used 21700 cells in Model 3, allowing for higher energy densities and significant cost reductions in production.[3] The Tesla 4680 cell also features a tabless design, further cutting production costs.[4] BYD relies on blade batteries, representing an innovative approach to battery technology. The aim is to produce long-lasting cells at a low cost and with high safety by utilizing a unique cell design.[5] Cell manufacturers typically publish only limited information in their datasheets for batteries. These datasheets provide measured performance data but need more scientific relevance due to missing details on testing conditions and insufficient data on charging limits and cell aging behavior.[6–8] Detailed information about the mechanical structure and cell characteristics is rarely published.

The development of LIBs for EVs focuses on optimizing cost, energy density, and power capability while maintaining other critical characteristics, such as safety and longevity.[9–11] Battery selection and design for EVs is a trade-off between these factors, with cost, energy density, and power capability being the essential requirements.[9–11] Different cell chemistries are suited for various applications: lithium iron phosphate (LFP) batteries are cost effective and offer longevity, making them suitable for affordable vehicle segments. In contrast, high-nickel chemistries like NMC811 provide superior energy density, making them ideal for higher performance and cost segments.[12] The choice between these chemistries depends on whether the focus is on cost, range, or performance.[12] In recent years, there has been a trend moving toward cells with larger dimensions, as it increases the energy content per cell produced and decreases the integration complexity at the system level.[3]

This article aims to build on the advancements in providing data on state-of-the-art battery cells used in automotive applications. Comparing a cost-focused cell design (the BYD Blade cell) with a performance-oriented cell design (Tesla 4680 cell) offers insights into their respective advantages and trade-offs.

The two cells of this article are examined for their mechanical, electrical, and material properties. The first cell is a cylindrical cell with a diameter of 46 mm and a height of 80 mm made by the manufacturer Tesla (Tesla 4680 cell) and used in the 2022 models of the Model Y class. The second cell is a prismatic

Please cite this article in press as: Gorsch et al., Contrasting a BYD Blade prismatic cell and Tesla 4680 cylindrical cell with a teardown analysis of design and performance, Cell Reports Physical Science (2025), https://doi.org/10.1016/j.xcrp.2025.102453

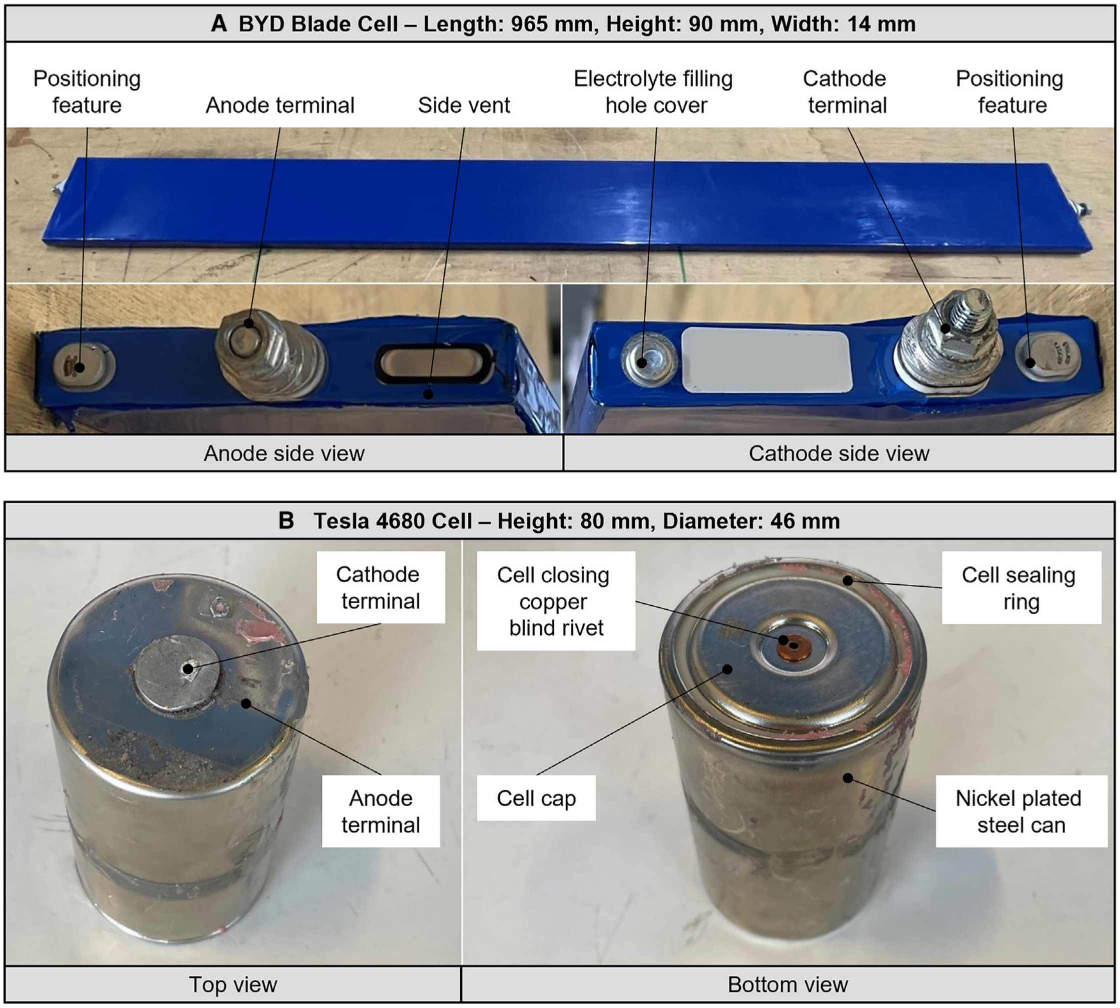

Figure 1. Cells' outside features, dimensions, and format
(A) BYD Blade cell.
(B) Tesla 4680 cell.

cell with dimensions of 90 mm in height, 965 mm in length, and 14 mm in thickness from the manufacturer BYD (BYD Blade cell). The Tesla 4680 cell was removed from the battery pack of a new 2022 version Tesla Model Y and distributed by Munro & Associates. As a result, the exact aging condition of the cell at the start of the article was uncertain but expected to be at 100% state of health (SOH). The BYD Blade cell was imported online from a China distributor with an SOH of 100% (in 2023).

This article aims to supplement the studies by Ank et al., Baazouzi et al., and Börner et al. with additional information on specific design or performance features of the Tesla 4680 cell and provide data on the BYD Blade cell design.[3,4,7] The article by Ank et al. is supplemented with additional information on specific geometry design features of the 4680 Tesla cell, such as the exact electrode positions in relation to the separator, and updated geometry parameters, such as the separator height. Furthermore, an extended focus is placed on the manufacturing processes and sequence, the exact material composition of the cell electrodes, and the respective material costs. The electrical behavior of the cell is supplemented by the temperature dependence of the internal direct current (DC) resistance.[6] Baazouzi et al.'s and Börner et al.'s studies are supplemented with a revised production sequence of the Tesla 4680 cell and additional data on design details, leading to a more detailed proposed production sequence for the cell assembly. Both studies are enriched by more detailed data on material composition and cost.[3,4] The overall focus of this article is also to directly compare differences in the mechanical design, production features, electrical behavior, and material composition of two automotive cells of different formats and design approaches to better understand the advantages and disadvantages of different cell design decisions.

To provide input for the next-generation design of prismatic or cylindrical LIBs, this article compares and analyzes the following:

(1) overall cell data, including outer dimensions and energy densities

Table 1. Overview of general cell properties and dimensions

	Tesla 4680 cell	BYD Blade cell
General		
Nominal capacity, Ah	23.125	135
Nominal energy, Wh	85.56	432
Nominal voltage, V	3.7	3.2
Voltage window, V	2.5–4.3	2.6–3.65
Weight	355 g	2.7 ± 0.3 kg
Volume, mL	133	1,216
Energy density (gravimetric), Wh/kg	241.01	160
Energy density (volumetric), Wh/l	643.3	355.263
The areal capacity of the cathode (calculated), mAh/cm^2	4.99	2.393
Dimensions		
Diameter/length, mm	46	965
Height, mm	80	90
Thickness, mm	–	14 mm
Can wall thickness (sides), mm	0.4	0.3
Separator, μm	10	12
Anode coating thickness, μm	125	65
Copper substrate foil thickness, μm	10	10
Cathode coating thickness, μm	75	70
Aluminum substrate foil thickness, μm	20	20
No. of separator layers	2	78
No. of cathode sheets (coating on both sides)	1	38
No. of anode sheets (coating on both sides)	1	39

(2) detailed mechanical design features and their respective implications for the cell assembly process
(3) material distribution across each cell component
(4) material costs
(5) exact dimensions of the cell electrodes
(6) process flow of cell assembly
(7) cell heating behavior and DC resistance
(8) detailed material composition of the electrodes, including the binders used

RESULTS AND DISCUSSION

This section will first focus on the cell's mechanical design and production process flow, then on the cell's electrical performance, and conclude with the material composition of the cell electrodes.

Mechanical design and production process

The main difference between the Tesla 4680 cell and BYD Blade cells is their formats: BYD uses a large prismatic cell format, while the Tesla 4680 cell is a large cylindrical cell with a significantly lower volume (Figure 1). Both cells exemplify the trend of increasing cell sizes and the cell-to-pack approach.[13–16] The BYD cell features threaded side terminals, allowing easily detachable cell-to-cell joints. The prismatic format is the only format that allows such joints.[17] Additionally, it includes pins on both sides, likely for mechanical positioning in a pack configuration. The BYD cell's aluminum housing is insulated with an adhesive polyethylene terephthalate (PET) foil, whereas the (presumably) nickel-plated steel can[18] of the Tesla 4680 cell lacks direct insulation at the cell housing level.

The Tesla 4680 cell utilizes NMC811 chemistry[7] (confirmed by energy-dispersive X-ray [EDX] results; Table S2), and the BYD Blade cell uses LFP chemistry (as specified by the cell datasheet and confirmed by EDX results; Table S3). The cells' capacities and nominal voltages were measured at C/10 constant current constant voltage (CCCV) charging and discharging cycles with a CV cutoff at a C/20 current, averaging the charging and discharging capacities of the cells. The voltage window was based on the limits of LFP and NMC811 with graphite anode cell chemistry. Comparing the cells on the cell level, the energy density of the Tesla 4680 cell outperforms that of the BYD Blade cell by margins of 1.5× gravimetrically and 1.8× volumetrically (Table 1). The applied cathode materials' (CAMs) experimentally achieved material-level energy densities are 720 Wh/kg for NMC811 and 528 Wh/kg for LFP.[19,20] When dividing the cell-level energy densities by these material-level energy densities, the CAM utilization rates are 33.45% for the Tesla 4680 cell and 30.3% for the BYD Blade cell. Therefore, both cells have a relatively close weight utilization of the CAM. This is significant because a larger cell typically allows for improved utilization due to a reduced fraction of passive components. The cathode areal capacity was calculated by dividing the nominal cell capacity by the total cathode coating area. Table 1 summarizes the main cell-level parameters.

Cell housing

Figure 2 displays a simplified sketch of the mechanical assemblies of both cells. In contrast to cylindrical cells like the 18650 and 21700 battery cells[21] and prismatic battery cells applied by Tesla,[22] the Tesla 4680 cell vents toward the cell's bottom, and the BYD Blade cell vents toward the side. This allows venting in case of failure away from the passenger and, in the case of the Tesla cell, away from the electrical contact system. The can of the Tesla 4680 cell has anode potential and functions as the negative terminal. Both polarities are insulated from the can for the BYD blade cell—the can sits at its own potential level. The electrolyte filling hole is closed via a copper blind rivet for the Tesla 4680 cell and welded shut for the BYD Blade cell. The Tesla 4680 cell cap/positive terminal is insulated with a sealing ring, while the BYD Blade cell terminals are insulated with plastic holders and a rubber O-ring.

Cell electrode configuration

The BYD Blade cell features a single Z-folded electrode stack with 38 double-coated cathode sheets, 39 double-coated anode sheets, and 79 separator layers (of one continuously folded separator sheet). The separator overhang is laminated—so that even the open sides of the Z-folded separator folds at the stack's long top and bottom sides are closed, presumably to fixate each cathode and anode sheet. On top of the laminated stack edge, a plastic rail is fixated via adhesive tape (Figure 3). The contacting assemblies at both ends are also fixed to the stack via adhesive tape. The whole stack and the plastic holders of the contacting assemblies are then wrapped in a transparent insulation bag.

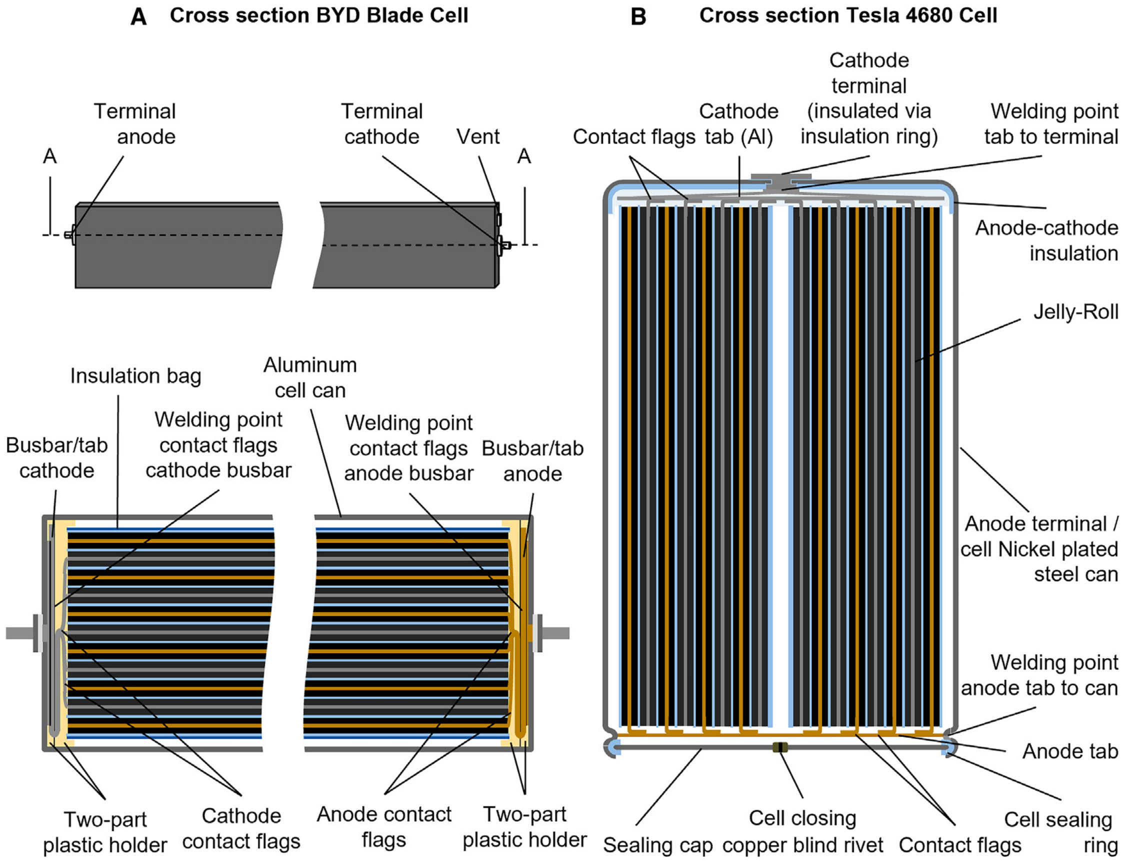

Figure 2. Simplified sketch of the cells' cross-sections displaying all internal components
(A) BYD Blade cell.
(B) Tesla 4680 cell.

The Tesla 4680 cell features a jelly roll configuration wrapped in the separator and then fixated via two strips of adhesive tape at the top and bottom (Figure 3). The center of the jelly roll is left empty and is presumably needed to contact the cathode tab to the cell terminal via a spot welding tool which is passed through this center cavity during production.

Contacting of the jelly roll/stack

The BYD Blade cell electrodes have typical contacting flags extending out of the stack. On both sides, they are welded to a busbar, which is, in turn, connected to the outside terminal. The contacting is done via two welding technologies: first, the contacting flags of the electrode layers are connected and compacted via ultrasonic welding, and in another step, the pre-connected flags are welded to the busbar via laser welding (Figure 4). The advantage of this approach is that laser welding only needs accessibility to the busbar from one side, and the ultrasonic welds ensure layer-to-layer contact in preparation for laser welding. This allows for a very space-efficient contacting design (Figure 2) where the contacting itself only takes the space of one electrode foil stack fold. The Tesla 4680 cell electrode/contacting foil edges (anode and cathode) are slit at an angle and then folded onto another, creating a contacting surface for the tabs. This so-called tabless design is showcased in Tesla's patent application for a tabless cell.[23] The exact geometries of the tabs can be found in Ank et al.'s study.[7] The tabs are welded onto the jelly roll via laser welding on six triangle-shaped contact surfaces (Figure 4). The cathode tab is spot welded to the terminal, and the anode tab is laser welded to the cell can.

Electrodes

The electrode dimensions were measured by disassembling the jelly roll stack in a glovebox and measuring the components using calipers and measuring tapes. A thin-film measuring device was used for layer and foil thickness measurements, and the average of 5 measurements was calculated to generate a representative layer or foil thickness. Figure 5 displays the electrode dimensions for both cells, and Table 1 presents the electrode thicknesses and the numbers of layers. Notably, the electrode foil thicknesses and the cathode coatings for both cells have similar thicknesses. On the anode coating side, the coating for the Tesla 4680 cell is almost twice as thick as that for the BYD Blade cell due to the higher specific energy of the cell's cathode. Both cells have a coating layer at the edges of the current collector flags—presumably an insulating coating layer to protect the edges of the electrodes from short circuits, as also detected by Ank et al.[7] The dimensions of the Tesla 4680 cell electrode

Please cite this article in press as: Gorsch et al., Contrasting a BYD Blade prismatic cell and Tesla 4680 cylindrical cell with a teardown analysis of design and performance, Cell Reports Physical Science (2025), https://doi.org/10.1016/j.xcrp.2025.102453

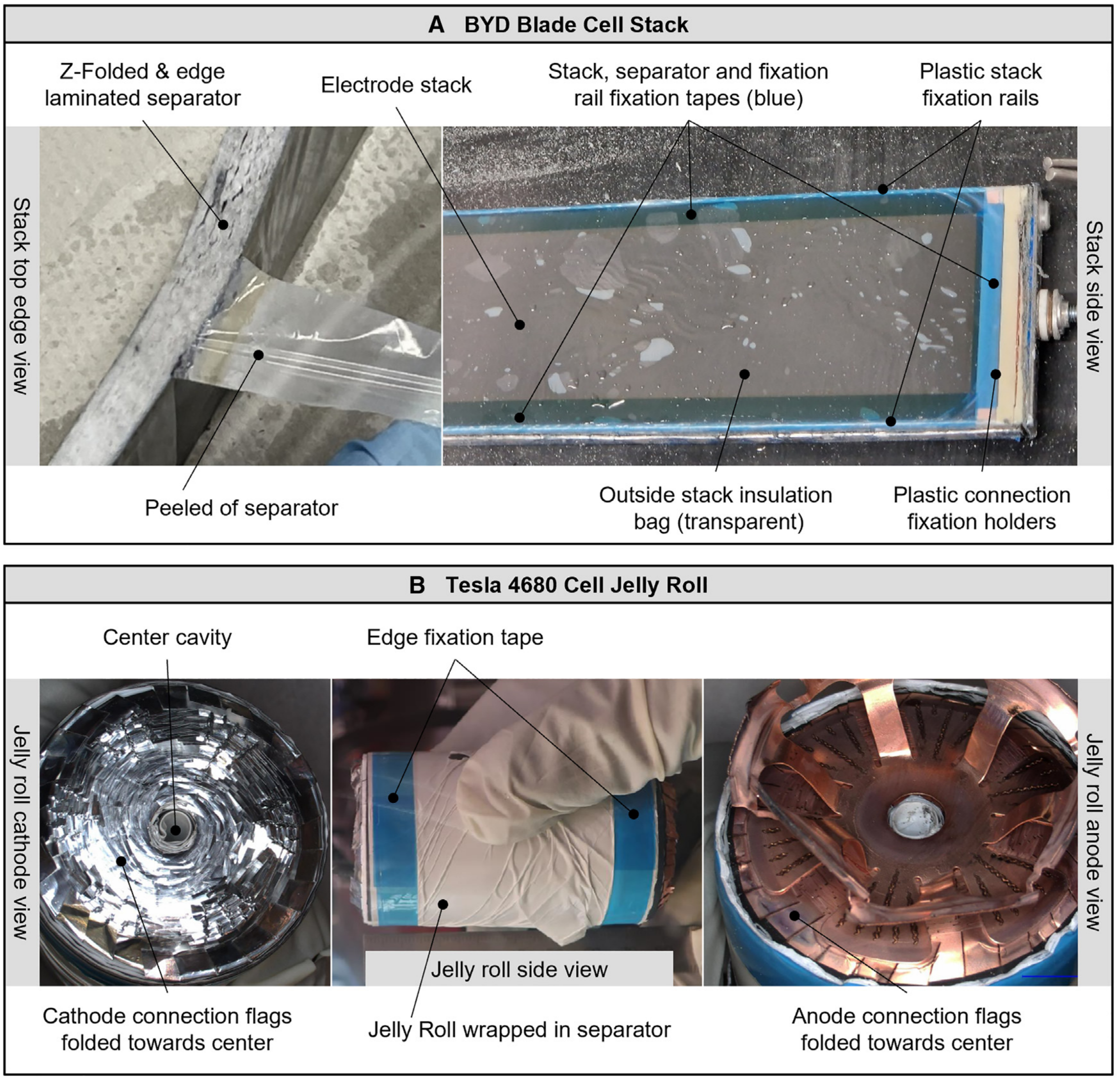

Figure 3. Pictures of the cells' internal electrode configurations and features
(A) BYD Blade cell stack.
(B) Tesla 4680 cell jelly roll.

display the relative positions of the electrodes before being rolled into the jelly roll configuration. The pathway for the current through the electrode foil in the BYD Blade battery electrodes is significantly longer than that in the Tesla 4680 battery cell electrodes. The overhang of the separator to the anode is 2 mm for the Tesla 4680 cell and the BYD Blade cell. The overhangs of the anode to the cathode are 1 mm for the Tesla 4680 cell and 1 mm for the BYD Blade cell.

Process flow

The manufacturing process flow for each cell was determined by analyzing the mechanical features and components of the cell and comparing them with the ideal process flows of prismatic and cylindrical cells as proposed by Heimes and Liu et al.[24,25] The process flow for electrode production and cell assembly for both types of cells is displayed in Figure 6. While the electrode production for both cells is expected to be similar, different production steps are utilized in cell assembly. The key differences include stack/jelly roll building processes (winding vs. Z-folding), electrode flag contacting, and cell closing technologies. The Tesla 4680 cell is sealed through an edge-bending process, whereas the BYD Blade cell requires multiple laser welding steps. Overall, the prismatic cell requires two more assembly steps. Still, the energy content per unit assembled is approximately five times higher, meaning that to achieve the same production output in kWh, BYD Blade cell production only needs to assemble one-fifth of the units.

Materials and material costs

To analyze the weight distribution of the cell, each component was weighed separately. The weight of larger components, such as the separator sheets, was determined by cutting and weighting 50 × 50 mm samples and calculating the total

Please cite this article in press as: Gorsch et al., Contrasting a BYD Blade prismatic cell and Tesla 4680 cylindrical cell with a teardown analysis of design and performance, Cell Reports Physical Science (2025), https://doi.org/10.1016/j.xcrp.2025.102453

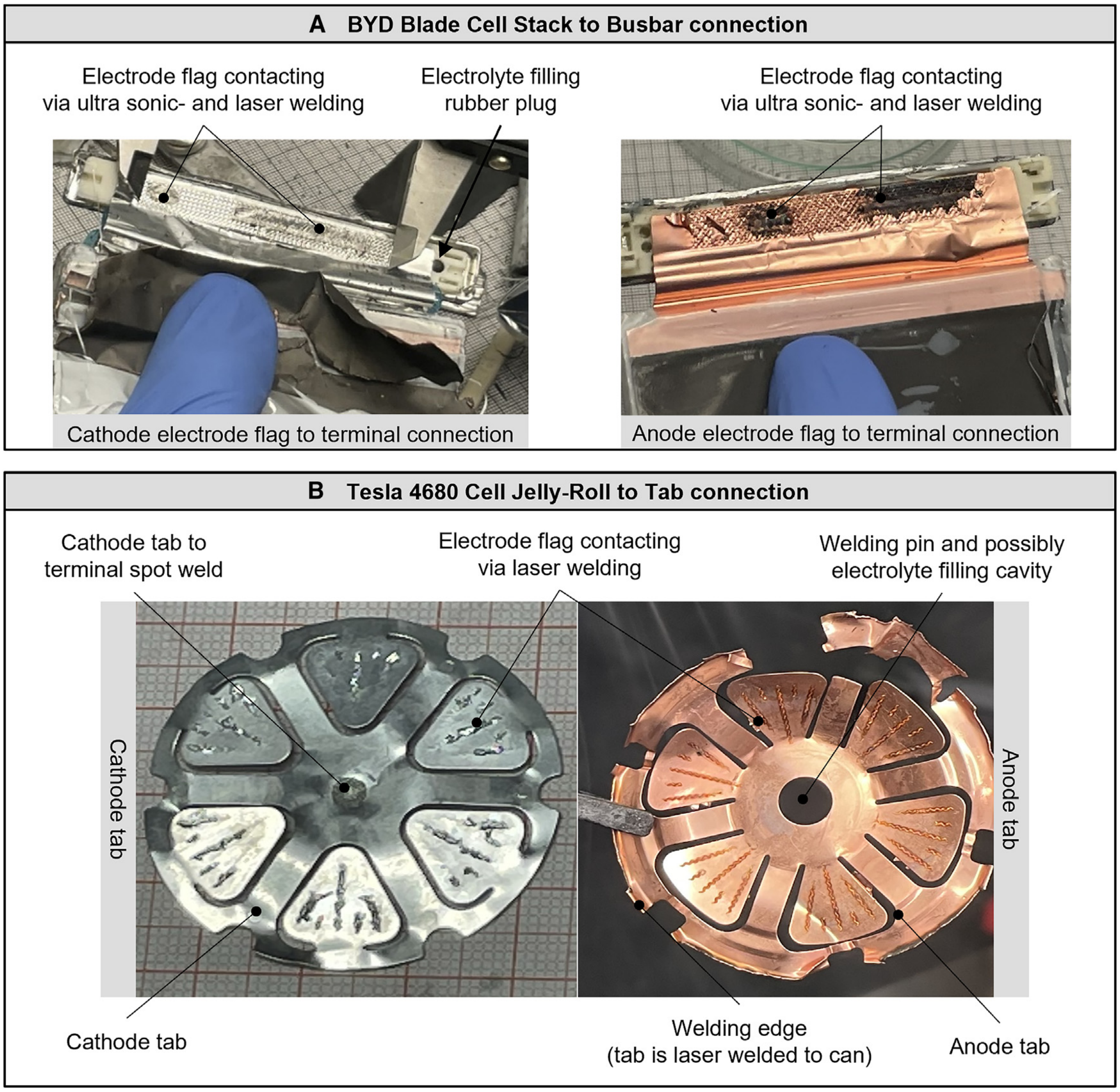

Figure 4. Pictures of the cells' internal electrical connection components and contacting technology
(A) BYD Blade cell.
(B) Tesla 4680 cell.

component weight based on the total component geometry. Notably, the steel housing of the Tesla 4680 cell constitutes a significantly larger proportion of the total cell weight compared to the BYD aluminum housing. However, this weight advantage is offset by the high substrate foil weight fractions of the BYD Blade cell, resulting in a similar fractions of active material weight of approximately 60% for both cells (Figure 7). Thus, for these cells, the advantage of larger battery cells having a smaller fraction of passive components is not apparent and heavily depends on the specific design choices for each cell. Material costs were estimated by accessing freely available material prices as of August 2024. Active material prices were approximated by dividing the material components and summing up the costs of the weight fractions of each component. The cost of CAM was determined via the summation of the costs of individual components (nickel manganese, cobalt, and lithium for NMC811 and iron oxide, phosphoric acid, and lithium for LFP) at the proportions calculated for the cells. For the anode active material (AAM), a 100% graphite content was assumed. The material cost per cell was then divided by the cell's energy to generate specific comparable €/kWh prices. The NMC-based CAMs significantly influence cost differentiation due to the high nickel and cobalt prices compared to iron oxide and phosphoric acid prices. Consequently, at current price levels, the €/kWh price of the larger BYD Blade cell is €10/kWh cheaper, highlighting the cost advantage of LFP batteries (Figure 7). Notably, the AAM cost per kWh for the BYD Blade cell is higher than that of the Tesla 4680 cell. The reason for this becomes apparent when the amount of AAM material per kWh is calculated. The BYD Blade cell relative AAM weighs

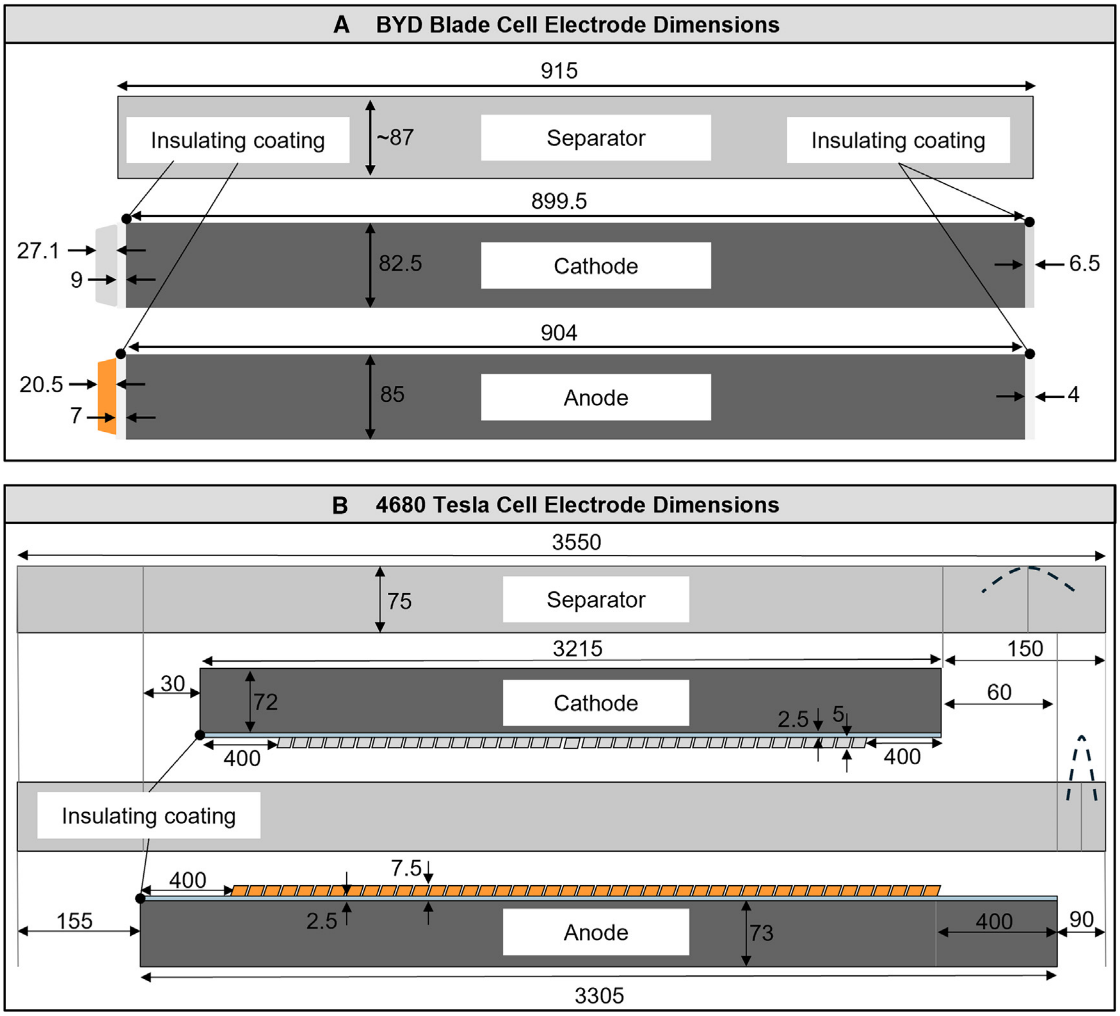

Figure 5. Dimensions and relative location of the cell's electrodes in mm
(A) BYD Blade cell.
(B) Tesla 4680 cell.

1.35 kg/kWh, and the Tesla 4680 cell relative AAM weighs 1.03 kg/kWh. This means that the Tesla cell utilizes a higher-energy-density AAM material or lower anode capacity-to-cathode capacity ratio (NP ratio).

Electrical performance

The cells' capacity and nominal voltage were measured at C/10 CCCV charging and discharging cycles with a constant voltage (CV) cutoff at a C/20 current, averaging the charging and discharging capacities of the cells (Table 1). The cells' efficiency behaviors were compared to evaluate the electrical performance of the cells.

Cell thermal efficiency

To compare the cell thermal efficiency, the cell internal DC resistance was characterized at 10% step state of charge (SOC) levels and 10°C, 20°C, and 40°C for both cells. The measurements were carried out according to standard ISO 12405-4.[29] The average charging and discharging DC resistances at 1 C are displayed in Figure 8. As is characteristic of LIBs, the cell resistance increases with lower temperatures for both cells.[30] The Tesla 4680 cell resistance increases at high SOC values, especially at low temperatures, whereas the BYD Blade cell resistance decreases with higher SOCs. The reason for this observation could be an increased charge transfer resistance in and at the surface of the anode due to a high lithium concentration, as these resistances tend to rise with increased SOC.[31] This needs to be investigated further; a rise in the total cell resistance at higher SOC is unusual, as the cathode and cathode surface charge transfer decreases with higher SOCs, offsetting the anode resistance increase.[30,31] To compare the cell's specific heating behavior, the following formula was used:

$$\frac{\text{heating}}{\text{volume}} = \frac{I_{at\ 1C}^{2} * R_{average}}{V_{Cell}}, \text{where } I = \text{current},$$
$$R = \text{internal resistance, and } V = \text{volume.}$$

Please cite this article in press as: Gorsch et al., Contrasting a BYD Blade prismatic cell and Tesla 4680 cylindrical cell with a teardown analysis of design and performance, Cell Reports Physical Science (2025), https://doi.org/10.1016/j.xcrp.2025.102453

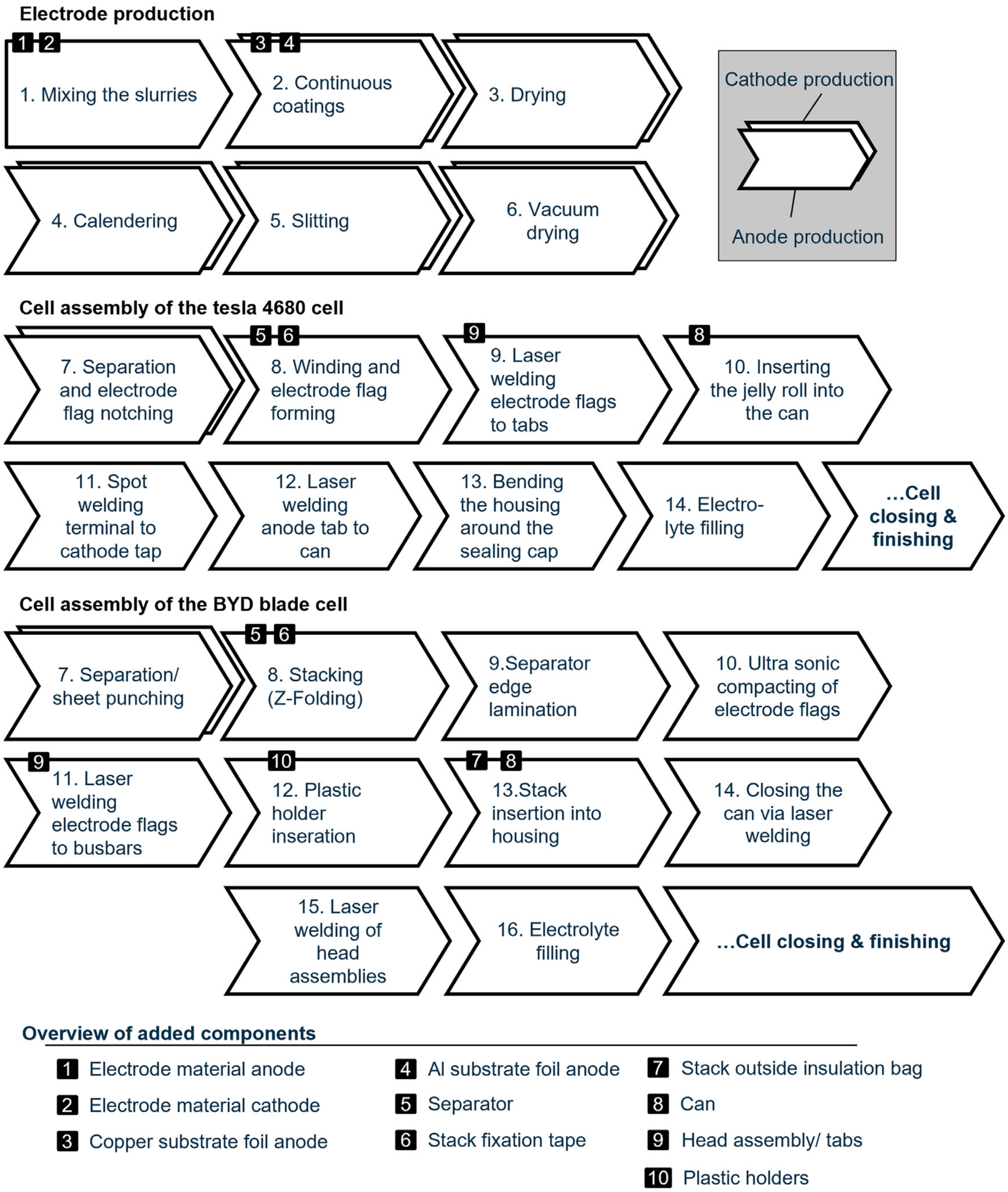

Figure 6. Tesla 4680 cell and BYD Blade cell assembly sequence proposal

Based on comparing the mechanical teardown analysis to the assembly sequences proposed by Heimes et al.[24] and Liu et al.[25]

Comparing this specific heating per volume, the Tesla 4680 cell creates around 2× of the heat to be dissipated at a 1 C load (Figure 8). Thus, when designing a system with the same power requirements, the cooling needed for the Tesla 4680 cells must dissipate approximately 2× more heat per volume than that needed for the BYD cell at the same load. Therefore, the LFP electrode design is more favorable for designing a cooling strategy for fast charging.

Electrode material investigations

To better understand the cell composition at a material level, both cells' positive and negative electrodes were investigated by scanning electron microscopy (SEM) and thermogravimetric analysis (TGA). Before any examinations, the electrodes were washed with dimethyl carbonate (DMC; anhydrous, purity: 99.5%, Sigma-Aldrich) solution three times to remove electrolyte residues from the surface.

Cell Reports
Physical Science
Article

CellPress
OPEN ACCESS

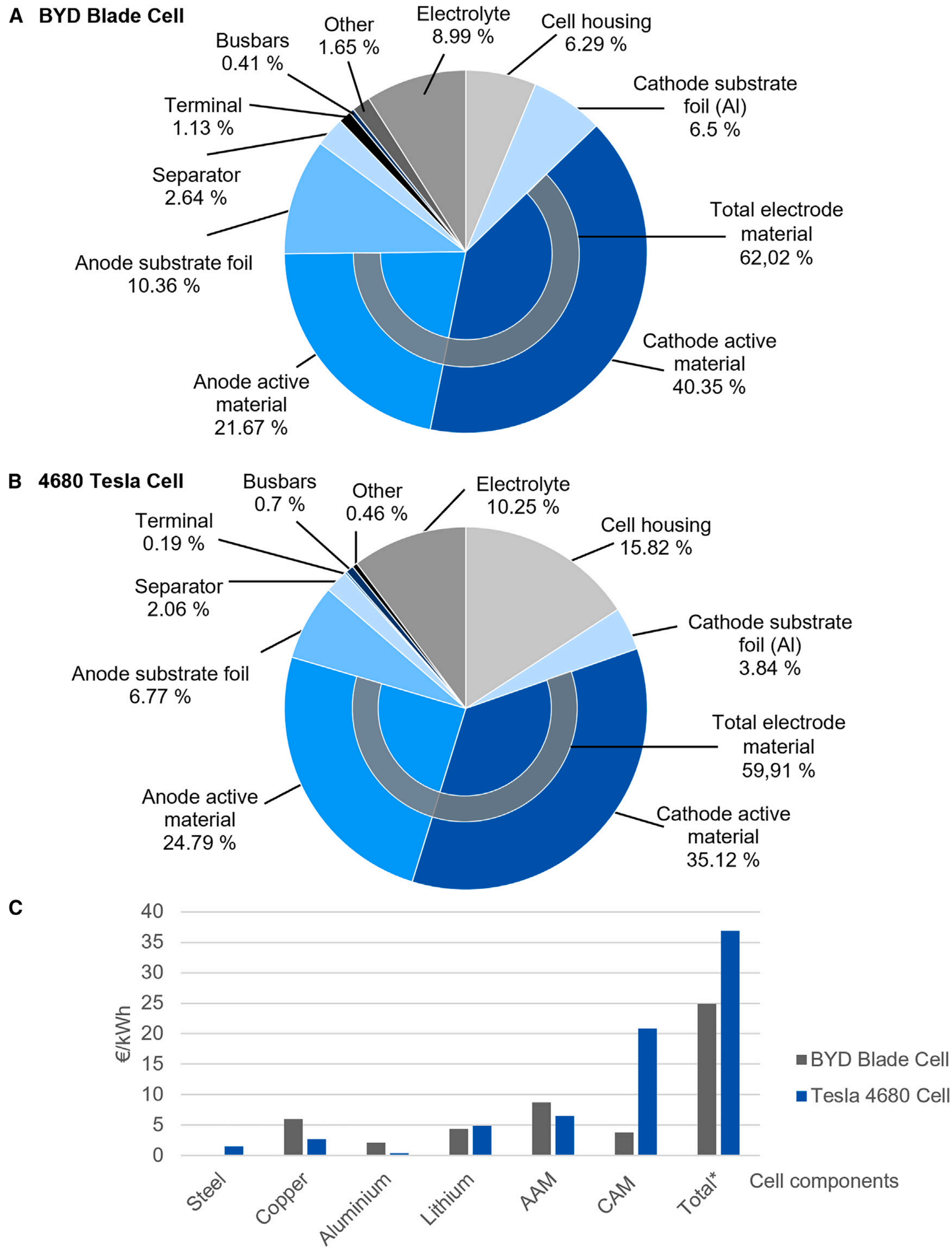

Figure 7. Cell component weight distribution and material cost

(A) BYD Blade cell.

(B) Tesla 4680 cell.

(C) Cell main component material cost × total cost without electrolyte and plastic components.[26–28]

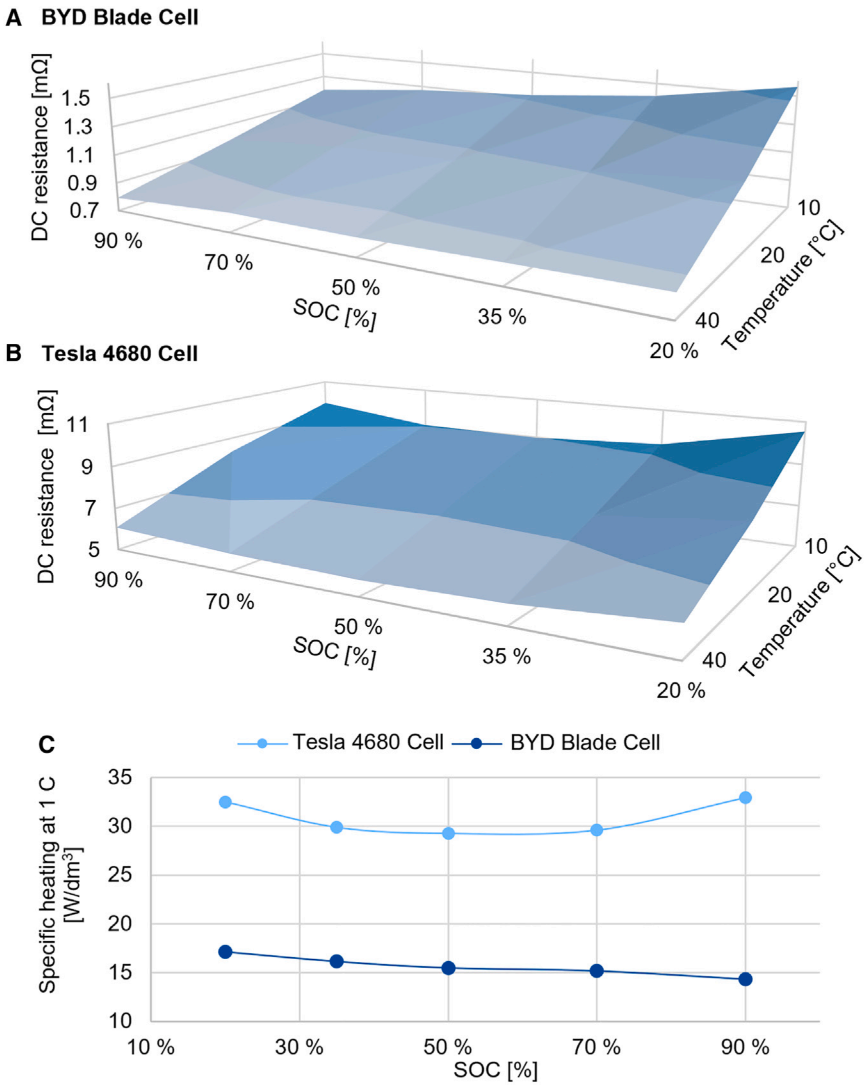

Figure 8. Average direct current resistance at 1 C 18 s charging and discharging pulses at 20°C and volume-specific heating of both cells at 1 C

(A) BYD Blade cell.

(B) Tesla 4680 cell.

(C) Volume-specific heating of both cells at 1 C.

Material characterization

SEM analysis allows a deeper look into the electrode morphology of both cells. In Tables S2 and S3, the element compositions of each electrode are listed. No Si or SiO_x was found in the electrodes, and while both anodes consist mainly of graphite, a substantial difference in particle morphology can be observed in Figure S1A. The primary particles of the BYD cell exhibit a flake-like structure. In the case of the Tesla anode, these particles have rounder edges and are bigger than in the BYD electrode. This means that the carbon material used in the BYD anode will have a higher surface area, suggesting the need for a higher binder content to maintain a stable network.[32]

Figure S1B compares the SEM images of both cathodes. The BYD cell cathode exhibits a distribution of nanometric LFP primary particles, some of them being aggregated in secondary particles of a few micrometers. This particle network includes small voids (pore-like cavities of a size less than 100 nm) and a significant amount of carbon nanotubes. These nanotubes can improve the conductivity of the LFP material and act as a binding agent between the particles. The Tesla cathode contains typical NMC spherical polycrystalline secondary particles about 10 μm in size, whose packing forms micrometric voids. This fits the trend of using polycrystalline in nickel-rich cathodes. Although single-crystal cathodes could have performance advantages, they pose challenges for the material synthetization process.[33] At the Tesla cathode's surface, the calendering process's effects are clearly visible since the spherical particles of the outer surface appear flattened.

Looking at the EDX results (Table S3), the relative material contents of the BYD Blade cell cathode reveal a typical LFP distribution comparable to the distribution detected by Stock et al. in a different automotive prismatic battery used by Tesla for Model 3 in China.[22] For the 4680 Tesla cell, a relative distribution of nickel manganese and cobalt correspondents with an 8:1:1 weight distribution (Ni, 81.6%; Mn, 6.4%; and Co, 12%), although the cobalt content is lower than 10%, confirming the results provided by Ank et al.[7] The high carbon content on the cathodes detected could be an indicator for conductive additives as well as carbon coatings of the material particle surface. The anode EDX results for both cells (Table S2) are very similar in carbon contents at roughly 90%. No silicon dioxide (SiOx) could be detected for either cell's anode.

Thermal analysis

Figure 9 displays the TGA performed on the anodes and cathodes of the cells. These curves illustrate the thermal stability of the electrodes. The derivative of the mass loss is plotted with dashed lines indicating at which temperatures mass loss occurs so that each peak can be attributed to a specific thermal decomposition reaction. It is observed that for both anode and cathodes, each cell material presents distinctive peaks that differ.

For instance, the BYD anode presents two peaks, which can be identified with the decomposition of carboxymethyl cellulose binder (CMC) between 200°C and 300°C and the decomposition of styrene butadiene rubber (SBR) at temperatures between 300°C and 450°C.[34] These may correspond with the usual water processing of graphite electrodes. However, the Tesla anode shows mass loss at different temperatures. In this case, two

Please cite this article in press as: Gorsch et al., Contrasting a BYD Blade prismatic cell and Tesla 4680 cylindrical cell with a teardown analysis of design and performance, Cell Reports Physical Science (2025), https://doi.org/10.1016/j.xcrp.2025.102453

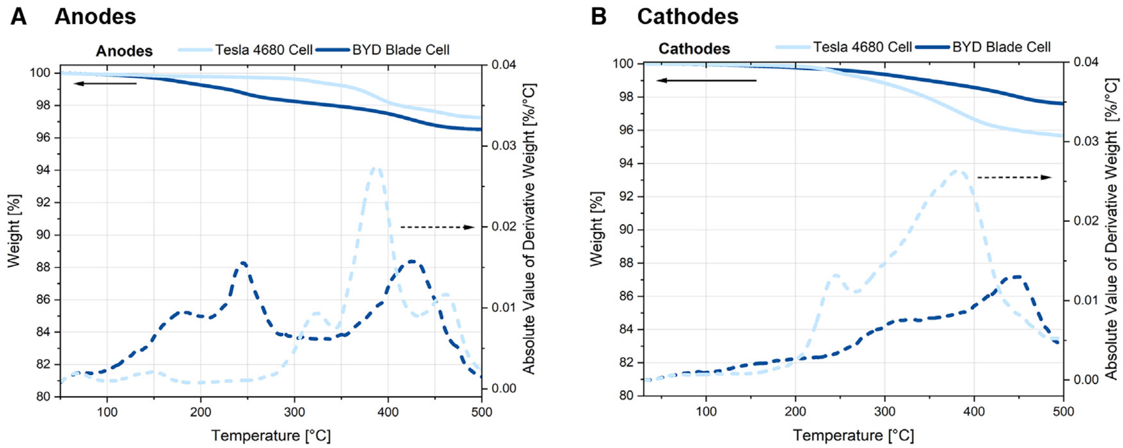

Figure 9. TGA investigations of anodes and cathodes
(A) Anodes.
(B) Cathodes.
Solid lines: weight loss of the samples; dashed lines: derivative weight of the samples; arrows indicate the corresponding axes.

different binders can be distinguished. The first mass decrease, between 300°C and 350°C, may correspond to the chain-splitting reaction of polyacrylic acid (PAA) polymer chains. In comparison, the weight loss around 450°C would fit the degradation of PAA polymer chains into monomers.[35] The more substantial peak at about 380°C is consistent with the degradation of polyethylene oxide (PEO).[36]

In the case of the cathode TGA curves, a slight mass loss occurs for the BYD LFP cathode between 400°C and 500°C. The loss can be attributed to the thermal decomposition of the polyvinylidene fluoride or polyvinylidene difluoride (PVdF) binder at this temperature range.[37] In comparison, the Tesla cathode displays degradation reactions at different temperatures, which would indicate the presence of other types of binders. For the NMC811 cathode, a slight mass decrease is observed between 200°C and 300°C and a steeper one between 300°C and 450°C. These two may correspond to the decomposition reactions of CMC and SBR. This would suggest that the Tesla cathode has followed an alternative fabrication process that differs from typical PVdF-N-methyl-2-pyrrolidone-based cathode processing.

This article provides insights into the design and characteristics of state-of-the-art LIBs for automotive applications. The comparative analysis of the Tesla 4680 cylindrical cell and the BYD Blade prismatic cell highlighted significant mechanical, electrical, and material differences that could influence future cell design iterations.

Key distinctions were observed in internal configurations, with cylindrical and prismatic cells necessitating different approaches to electrode contacting. The results showed that laser welding could be effectively applied in these processes for both cell formats. Additionally, the material composition of the cells, including the active materials, electrode structures, and binders, was analyzed, presenting a basis for future resource and process analysis. The findings also contribute to potential enhancements in battery thermal management or efficiency improvements on the cell level, given the differences in internal heating behaviors between the cells.

This article provides data on these two cells' material compositions, process flows, and electrical performances, offering a base for further research and industry applications. It also raises questions for future investigations, particularly regarding the binder formulations observed in Tesla's 4680 cells, which may represent an area for further exploration. As both Tesla and BYD continue to innovate and improve their battery technologies, the findings of this article will serve as a benchmark for future developments in automotive battery design.

METHODS

The experiments conducted for the mechanical and electrical characterization of the cells are presented in this section. Both cells were electrically characterized utilizing the AMETEK SI-9300R Battery Analyzer and tested within a Weisstechnik climate chamber, only controlling temperature for the tests. The electrical contacting units were designed with more than a 1.5× current safety factor for the contacting components. All measurements were conducted using four-point sensing (separation of sense and power cables) using shielded cables. The cells were dismantled using mechanical tools and visually and geometrically inspected within an argon environment MBraun glovebox. To open the Tesla 4680 cell, a Dremel with a diamond disc was used, and the cut was made right at the top and bottom edges of the cell can. The BYD Blade cell was opened at multiple incision points using pliers. The cells were discharged to 0% SOC before disassembly with a CCCV 0.1 C discharge procedure utilizing the AMETEK SI-9300R Battery Analyzer. Electrode probes were taken and sealed into pouch foils under an argon environment for later material analysis. All electrode probes were cut out with a ceramic knife or ceramic scissors. To avoid particle contamination of the electrode samples, samples were only cut out from inner electrode sections.

The electrodes' particle morphology and surface topography were investigated via SEM (Carl Zeiss AURIGA). An acceleration voltage of 3 kV was used for surface analysis and 15–20 kV for

EDX analysis. EDX was performed using an X-max 80 mm^2 detector, and the data were evaluated with INCA software (Oxford Instruments).

TGA was performed using an SDT IR Q500 from TA Instruments. 5 mm samples were punched and transferred to a platinum pan. The temperature was equilibrated at 30°C for 40 min in an isothermal step with a helium balance flow rate of 30 mL min^{-1} and a mass flow of 10 mL min^{-1}. Measurements were performed with a heating rate of 5 K min^{-1} up to 500°C.

RESOURCE AVAILABILITY

Lead contact

Further information and requests for resources and reagents should be directed to and will be fulfilled by the lead contact, Jonas Gorsch (j.gorsch@pem.rwth-aachen.de).

Materials availability

This study did not generate new unique reagents.

Data and code availability

- Data: generated data on cell electrical behavior or mechanical properties reported in this paper will be shared by the lead contact upon request.
- Code: this paper does not report original code.
- All other items: any additional information required to reanalyze the data reported in this paper is available from the lead contact upon request.

ACKNOWLEDGMENTS

This research was funded by the German Federal Ministry of Education and Research (grant no. 03XP0256). The authors also acknowledge Debbie Stappers for TGA measurements, Lara Kersting for EDX data processing, Lennart Alsheimer for sample preparation, and Matthias Konersmann for research support.

AUTHOR CONTRIBUTIONS

Conceptualization, J.G., J.S., M.M.-C., and E.S.; investigation, writing – original draft, J.G. and M.M.-C.; writing – review and editing, M.F., D.K., and N.K.; funding acquisition, H.H. and A.K.; supervision M.F., H.H., and A.K.

DECLARATION OF INTERESTS

The authors declare no competing interests.

SUPPLEMENTAL INFORMATION

Supplemental information can be found online at https://doi.org/10.1016/j.xcrp.2025.102453.

Received: September 25, 2024
Revised: November 25, 2024
Accepted: January 27, 2025
Published: March 6, 2025

REFERENCES

1. Impey, B. (2024). Anzahl verkaufter Elektroautos weltweit nach Marken im Jahr 2023. https://de.statista.com/statistik/daten/studie/561568/umfrage/die-groessten-hersteller-von-elektroautos-nach-absatz/.
2. Chen, C. (2024). BYD Set to Challenge Tesla for the Crown in EV Sales in 2024. Says TrendForce. https://www.trendforce.com/presscenter/news/20240220-12030.html.
3. Baazouzi, S., Feistel, N., Wanner, J., Landwehr, I., Fill, A., and Birke, K.P. (2023). Design, Properties, and Manufacturing of Cylindrical Li-Ion Battery Cells—A Generic Overview. Batteries *9*, 309. https://doi.org/10.3390/batteries9060309.
4. Börner, M.F., Mohsseni, A.M., De, N., Faber, M., Krause, F., Li, W., Bihn, S., Ringbeck, F., and Sauer, D.U. (2024). Manufacturing cost comparison of tabless vs. standard electrodes for cylindrical lithium-ion batteries. J. Energy Storage *77*, 109941. https://doi.org/10.1016/j.est.2023.109941.
5. BYD Press Release. BYD's revolutionary Blade Battery: all you need to know. https://www.byd.com/eu/blog/BYDs-revolutionary-Blade-Battery-all-you-need-to-know.html.
6. Ank, M., Kröger, T., Schreiber, M., and Lienkamp, M. (2023). Experimental analysis of lithium-ion cell procurement: Quality differences, correlations, and importance of cell characterization. J. Energy Storage *66*, 107430. https://doi.org/10.1016/j.est.2023.107430.
7. Ank, M., Sommer, A., Abo Gamra, K., Schöberl, J., Leeb, M., Schachtl, J., Streidel, N., Stock, S., Schreiber, M., Bilfinger, P., et al. (2023). Lithium-Ion Cells in Automotive Applications: Tesla 4680 Cylindrical Cell Teardown and Characterization. J. Electrochem. Soc. https://doi.org/10.1149/1945-7111/ad14d0.
8. Günter, F.J., and Wassiliadis, N. (2022). State of the Art of Lithium-Ion Pouch Cells in Automotive Applications: Cell Teardown and Characterization. J. Electrochem. Soc. *169*, 30515. https://doi.org/10.1149/1945-7111/ac4e11.
9. Das, D., Gope, S., Jana, M., and Basu, S. (2021). Cell Selection Based on Chemistry and Key Parameters for Electric Vehicle. In 2021 IEEE Transportation Electrification Conference (ITEC-India), pp. 1–7. https://doi.org/10.1109/ITEC-India53713.2021.9932540.
10. Schmuch, R., Wagner, R., Hörpel, G., Placke, T., and Winter, M. (2018). Performance and cost of materials for lithium-based rechargeable automotive batteries. Nat. Energy *3*, 267–278. https://doi.org/10.1038/s41560-018-0107-2.
11. Miao, Y., Hynan, P., von Jouanne, A., and Yokochi, A. (2019). Current Li-Ion Battery Technologies in Electric Vehicles and Opportunities for Advancements. Energies *12*, 1074. https://doi.org/10.3390/en12061074.
12. Hasselwander, S., Meyer, M., and Österle, I. (2023). Techno-Economic Analysis of Different Battery Cell Chemistries for the Passenger Vehicle Market. Batteries *9*, 379. https://doi.org/10.3390/batteries9070379.
13. Link, S., Neef, C., Wicke, T., Hettesheimer, T., Diehl, M., Krätzig, O., Degen, F., Klein, F., Fanz, P., and Burgard, M., et al. (2022). Development perspectives for lithium-ion battery cell formats (Fraunhofer ISI). https://doi.org/10.24406/publica-1321.
14. Gerlitz, E., Botzem, D., Weinmann, H., Ruhland, J., and Fleischer, J. (2021). Cell-to-Pack-Technologie für Li-Ionen-Batterien. Zeitschrift für wirtschaftlichen Fabrikbetrieb *116*, 689–694. https://doi.org/10.1515/zwf-2021-0146.
15. Kampker, A., Heimes, H.H., Offermanns, C., Vienenkötter, J., and Robben, T. (2023). Framework and Classification of Battery System Architectures. WEVJ *14*, 88. https://doi.org/10.3390/wevj14040088.
16. Löbberding, H., Wessel, S., Offermanns, C., Kehrer, M., Rother, J., Heimes, H., and Kampker, A. (2020). From Cell to Battery System in BEVs: Analysis of System Packing Efficiency and Cell Types. WEVJ *11*, 77. https://doi.org/10.3390/wevj11040077.
17. Das, A., Li, D., Williams, D., and Greenwood, D. (2018). Joining Technologies for Automotive Battery Systems Manufacturing. WEVJ *9*, 22. https://doi.org/10.3390/wevj9020022.
18. Bree, G., Horstman, D., and Low, C.T.J. (2023). Light-weighting of battery casing for lithium-ion device energy density improvement. J. Energy Storage *68*, 107852. https://doi.org/10.1016/j.est.2023.107852.
19. Nitta, N., Wu, F., Lee, J.T., and Yushin, G. (2015). Li-ion battery materials: present and future. Mater. Today *18*, 252–264. https://doi.org/10.1016/j.mattod.2014.10.040.

20. Savina, A.A., and Abakumov, A.M. (2023). Benchmarking the electrochemical parameters of the LiNi0.8Mn0.1Co0.1O2 positive electrode material for Li-ion batteries. Heliyon *9*, e21881. https://doi.org/10.1016/j.heliyon.2023.e21881.

21. Yao, X.-Y., Kong, L., and Pecht, M.G. (2020). Reliability of Cylindrical Li-ion Battery Safety Vents. IEEE Access *8*, 101859–101866. https://doi.org/10.1109/ACCESS.2020.2997792.

22. Stock, S., Hagemeister, J., Grabmann, S., Kriegler, J., Keilhofer, J., Ank, M., Dickmanns, J.L., Schreiber, M., Konwitschny, F., Wassiliadis, N., et al. (2023). Cell teardown and characterization of an automotive prismatic LFP battery. Electrochim. Acta *471*, 143341. https://doi.org/10.1016/j.electacta.2023.143341.

23. Tsuruta, K., Dermer, M.E., and Dhiman, R. (2020). Cell with a tabless electrode. Patent WO2020096973A1.

24. Heimes, H.H., Kampker, A., Wennemar, S., Plocher, L., Bockey, G., Michaelis, S., and Schütrumpf, J. (2023). Production process of a lithium-ion battery cell. https://www.pem.rwth-aachen.de/global/show_document.asp?id=aaaaaaaabyilawq.

25. Liu, Y., Zhang, R., Wang, J., and Wang, Y. (2021). Current and future lithium-ion battery manufacturing. iScience *24*, 102332. https://doi.org/10.1016/j.isci.2021.102332.

26. Statista GmbH (2024). https://de.statista.com/.

27. finanzen.net GmbH (2024). https://www.finanzen.net/.

28. Shanghai Metals Market (2024). https://www.metal.com/price.

29. International Organization for Standardization (2018). Electrically propelled road vehicles — Test specification for lithium-ion traction battery packs and systems —: Part 4: Performance testing. https://www.iso.org/standard/71407.html

30. Hossain Ahmed, S., Kang, X., and Bade Shrestha, S.O. (2015). Effects of Temperature on Internal Resistances of Lithium-Ion Batteries. J. Energy Resour. Technol. *137*, 031901. https://doi.org/10.1115/1.4028698.

31. Wu, M.-S., Chiang, P.-C.J., and Lin, J.-C. (2005). Electrochemical Investigations on Advanced Lithium-Ion Batteries by Three-Electrode Measurements. J. Electrochem. Soc. *152*, A47. https://doi.org/10.1149/1.1825385.

32. Weichert, A., Göken, V., Fromm, O., Beuse, T., Winter, M., and Börner, M. (2022). Strategies for formulation optimization of composite positive electrodes for lithium ion batteries based on layered oxide, spinel, and olivine-type active materials. J. Power Sources *551*, 232179. https://doi.org/10.1016/j.jpowsour.2022.232179.

33. Chen, Y.-S., Dominko, R., Marczewski, M., and Wieczorek, W. (2024). Optimizing high-energy lithium-ion batteries: a review of single crystalline and polycrystalline nickel-rich layered cathode materials: performance, synthesis and modification. Appl. Phys. *130*, 740. https://doi.org/10.1007/s00339-024-07897-7.

34. Stenzel, Y.P., Börner, M., Preibisch, Y., Winter, M., and Nowak, S. (2019). Thermal profiling of lithium ion battery electrodes at different states of charge and aging conditions. J. Power Sources *433*, 226709. https://doi.org/10.1016/j.jpowsour.2019.226709.

35. Lu, X., Tan, C.Y., Xu, J., and He, C. (2003). Thermal degradation of electrical conductivity of polyacrylic acid doped polyaniline: effect of molecular weight of the dopants. Synth. Met. *138*, 429–440. https://doi.org/10.1016/S0379-6779(02)00471-X.

36. Jakić, M., Vrandečić, N.S., and Klarić, I. (2013). Thermal degradation of poly(vinyl chloride)/poly(ethylene oxide) blends: Thermogravimetric analysis. Polym. Degrad. Stabil. *98*, 1738–1743. https://doi.org/10.1016/j.polymdegradstab.2013.05.024.

37. Javed, A., Makvandi, A., Demelash, F., Adhitama, E., Heidrich, B., Peterlechner, M., Wilde, G., Winter, M., and Börner, M. (2024). Interphase design of LiNi 0.6 Mn 0.2 Co 0.2 O 2 as positive active material for lithium ion batteries via Al 2 O 3 coatings using magnetron sputtering for improved performance and stability. Batteries & Supercaps *7*. https://doi.org/10.1002/batt.202300580.